
GeoBench: Benchmarking and Analyzing Monocular Geometry Estimation Models

Yongtao Ge^{1,2}, Guangkai Xu¹, Zhiyue Zhao¹, Libo Sun²,
Zheng Huang¹, Yanlong Sun³, Hao Chen¹, Chunhua Shen¹

¹ Zhejiang University ² The University of Adelaide ³ Tsinghua University

Code & Benchmark: <https://github.com/aim-uofa/GeoBench>

Abstract

Recent advances in discriminative and generative pretraining have yielded geometry estimation models with strong generalization capabilities. While discriminative monocular geometry estimation methods rely on large-scale fine-tuning data to achieve zero-shot generalization, several generative-based paradigms show the potential of achieving impressive generalization performance on unseen scenes by leveraging pre-trained diffusion models and fine-tuning on even a small scale of synthetic training data. Frustratingly, these models are trained with different recipes on different datasets, making it hard to find out the critical factors that determine the evaluation performance. Besides, the current widely used geometry evaluation benchmarks have two main drawbacks that may prevent the development of the field, *i.e.*, *limited scene diversity* and *unfavorable label quality*. To resolve the above issues, (1) we **build fair and strong baselines in a unified codebase** for evaluating and analyzing the state-of-the-art (SOTA) geometry estimation models in terms of both different finetuning paradigms and training recipes; (2) we **evaluate monocular geometry estimators on more challenging benchmarks** for geometry estimation task with diverse scenes and high-quality annotations.

Our results reveal that pre-trained using large data, discriminative models such as DINOv2, can outperform generative counterparts with **a small amount of high-quality synthetic training data** under the same training configuration, which suggests that fine-tuning data quality is a more important factor than the data scale and model architecture. Our observation also raises a question: if simply fine-tuning a general vision model such as DINOv2 using a small amount of synthetic depth data produces SOTA results, *do we really need complex models, e.g., Marigold [KOH⁺24] and DepthFM [GFP⁺24] for depth estimation?* We believe that this work can propel advancements in geometry estimation tasks and a wide range of other downstream vision tasks.

1 Introduction

Monocular depth and surface normal estimation, also referred to as “monocular geometry estimation”, poses a fundamental yet intricate challenge of inferring distance and surface orientation from a single image. Its significance is underscored by its broad utility across various downstream tasks, including object detection [HWSH22, WYK⁺20, DHY⁺20], visual navigation [TTLN17, YSWC20, SYX⁺22, YWSC18], novel view synthesis [DLZR22, RBM⁺22], controllable image generation [ZRA23, ECA⁺23, ZCC⁺24], and 3D scene reconstruction [SXC⁺21, DT20]. The importance of this task has led to a significant body of research, resulting in numerous models [BWM23, YKH⁺24, YZC⁺23, HYZ⁺24, KOH⁺24] over the past decade.

Although a large number of monocular geometry estimation models exist, they can be divided into two paradigms, *i.e.*, discriminative-based and generative-based. Most contemporary discriminative monocular geometry estimation models leverage the pre-train priors from fully-supervised image classification backbones, *e.g.*, ConvNeXt [WDH⁺23], EfficientNet [TL19] and ViT [DBK⁺20], or self-supervised backbones. *e.g.*, DINOv2 [ODM⁺24], previous best discriminative depth estimation models scale-up their performance with pre-trained DINOv2 backbone and *a large scale of fine-tuning data*. Generative geometry estimation models [KOH⁺24, FYH⁺24, XGL⁺24, GFP⁺24, LTLY24] unleash the power of pre-trained text-to-image diffusion models, *e.g.*, Stable Diffusion (SD) [RBL⁺22]. Several generative geometry estimation models [KOH⁺24, FYH⁺24, XGL⁺24, GFP⁺24] show strong generation capability with even *a small-scale high-quality synthetic fine-tuning data*.

However, none of the previous works have systematically investigated the performance of these geometry estimation methods with fair and faithful comparison. The reason is twofold. Firstly, *the different selections of datasets and training configurations hinder the fair evaluations of the newly designed methodologies*. (1) The performance distinction for different generative-based finetuning paradigms is unclear. It is hard to evaluate whether the actual improvement is from the algorithmic perspective or the data perspective since they are trained on different datasets and different training configurations. (2) The performance distinction between discriminative and generative geometry estimation models when trained on the same scale and quality of data also remains unclear. Secondly, *existing popular geometry estimation benchmarks may not reveal the real performance of the models*. NYUv2 [SHKF12] and ScanNet [DCS⁺17] are still popular in the evaluation of indoor monocular depth estimation. However, they are collected by an older Kinect-v1 system with noisy depth measurements and noisy imaging for RGB patterns, with only 640×480 resolution. DIODE [VKZ⁺19] and ETH3D [SSG⁺17] collect both outdoor and indoor scenes with high-quality data while with low diversity scenes for evaluation. KITTI [GLU12] collects depth maps from the LIDAR sensor and focuses on outdoor driving scenes. For surface normal evaluation, NYUv2 [SHKF12], ScanNet [DCS⁺17], iBims-1 [KLFK18], Sintel [BWSB12] and Virtual KITTI [GWCV16] are widely used by generating surface normal maps from the ground truth depth maps. However, the depth noises in NYUv2 [SHKF12], ScanNet [DCS⁺17] and iBims-1 [KLFK18] yield unsatisfactory surface normal ground truth. The limited scene diversity of synthetic datasets, *i.e.*, Sintel [BWSB12] and Virtual KITTI [GWCV16], cannot evaluate the robustness of the surface normal estimation model for in-the-wild geometry reconstruction. Overall, the existing geometry benchmarks are hindered by two main issues: ground-truth quality and scene diversity. This lack of fair and comprehensive benchmarks can significantly impede the development of geometry estimation research.

To address the aforementioned problems, we perform a comprehensive geometry estimation benchmarking study from two perspectives:

1. **Training strategy.** We reimplement a comprehensive list of SOTA algorithms in a unified codebase, including Marigold [KOH⁺24], Geowizard [FYH⁺24], GenPercept [XGL⁺24], DepthFM [GFP⁺24], DMP [LTLY24], Depth-Anything [YKH⁺24] and DSINE [BD24]. As such, we can fairly evaluate their performance under the same training configuration, and figure out whether the performance improvement is coming from the model architecture or coming from the high-quality training data. Previous generative geometry models are all based on Stable Diffusion 2.1 [RBL⁺22] with limited trained data (compared to the data scale of discriminative models), we further explore the potential of generative geometry models by conducting data scale-up and model scale-up ablations.
2. **More benchmark datasets.** Apart from traditional geometry evaluation benchmarks, we build more diverse scenes with high-quality labels for geometry evaluation. For depth estimation, we introduce three extra benchmark datasets, InSpaceType [WGH⁺23], MatrixCity [LJX⁺23], and Infinigen [RLM⁺23]. InSpaceType is an indoor depth evaluation benchmark, which contains 12 scenes, 1260 images, and 2208×1242 resolution. It is a good complement for indoor benchmarks like NYUv2 and ScanNet. MatrixCity is a rendered dataset with real city-scale scenes, we select 808 street images and 403 aerial images for evaluation. It is suitable for evaluating driving and city scenes. Infinigen is also a high-quality rendered dataset, which contains diverse nature scenes. We use it to verify the generalization capability of depth estimation foundation models in wild scenes. For surface normal estimation, we expand existing benchmark datasets with more high quality and

diverse datasets, *e.g.*, indoor MuSHRoom dataset [RWC⁺24], outdoor Tank and Temples (T&T) dataset [KPZK17]¹, and wild Infinigen [RLM⁺23] dataset.

With the unified codebase, training data, and comprehensive benchmark datasets, we surprisingly find that:

1. Without bells and whistles, the depth estimation model pre-trained on the DI-NOv2 [ODM⁺24] backbone, followed by a simple DPT head [RBK21], can already achieve great generalization performance by using only a small amount of high-quality synthetic datasets (77K training samples).
*With the same training configuration, the discriminative model outperforms the recent generative counterpart, Marigold [KOH⁺24]. Besides, the result is a sharp contrast to previous discriminative models using large data to achieve generalization capability, *e.g.*, Metric3Dv2 [HYZ⁺24], which focuses on collecting more diverse training datasets (16M training samples), and Depth-Anything [YKH⁺24], which focuses on scaling up model performance with large-scale pseudo labels (63.5M training samples). Based on the result, we argue that training data quality may be more important than the data scale.*
2. Generative-based geometry estimation models can generate high-resolution and detailed depth and surface normal maps, which is an advantage over the existing discriminative depth estimation models. We mainly attribute this to high-quality synthetic fine-tuning data and the design of the VAE [KW14] decoder, which can decode compressed depth latent to the same resolution depth map as the input image.
3. For surface normal estimation, the discriminative model DSINE [BD24] outperforms generative-based fine-tuning protocols with the same training configuration, suggesting that, apart from large-scale pre-training, inductive bias [BD24] can also be an important factor in providing rich information for surface normal estimation tasks.

We hope that our benchmarking results can pave the way for designing more powerful geometry estimation algorithms and developing more high-quality geometry estimation training datasets in the future.

2 Preliminaries

Task definition. Given an input image $x \in \mathbb{R}^{H \times W \times 3}$, the goal of monocular geometry estimation is to predict the depth map $d \in \mathbb{R}^{H \times W}$, which can be affine-invariant or metric depth, and surface orientation, which can be represented as either a unit vector $\mathbf{n} \in S^2$, or a 3D *axis-angle* $\mathbf{R} \in SO(3)$.

Discriminative geometry estimation models. With the widespread application of deep learning [LBH15], learning-based methods have demonstrated their ability to estimate geometric information from monocular images [EPF14, GMAFB19, RLH⁺22, YKH⁺24]. Early works primarily relied on discriminative models using either supervised or unsupervised methods. Eigen et al. [EPF14] proposed the first learning-based method for monocular depth estimation, employing two deep network stacks and using ground truth depth for supervision. Zhou et al. proposed an early unsupervised framework, SfMLearner [ZBSL17], in which camera pose and monocular depth are learned together. With the availability of large amounts of data, recent methods [RLH⁺22, YKH⁺24, YZC⁺23, HYZ⁺24] have shown a trend toward using large-scale datasets to develop robust geometry estimation models that generalize well to diverse environments. For instance, Ranftl et al. [RLH⁺22] introduced a method that demonstrates strong zero-shot testing ability by utilizing mixed training datasets. Yang et al. [YKH⁺24] further improved zero-shot monocular depth estimation performance by proposing Depth-Anything, which leverages large-scale data to achieve strong generalization ability. Meanwhile, Yin et al. [YZC⁺23, HYZ⁺24] proposed Metric3D, which can output accurate metric depth by training models on 11 public RGB-D datasets. Apart from depth estimation, advancements in surface normal information have also been achieved through the use of discriminative models. Surface normal information can not only be calculated directly from depth maps but can also be independently obtained through surface normal estimation techniques [WFG15, LZP14, LOM20, BD24]. For example, Bae et al. [BD24] proposed a method that demonstrates strong generalization capabilities and produces high-quality surface normal predictions by investigating inductive biases. Overall, the use

¹The surface normal annotation of MushRoom and T&T are obtained from Gaustudio [YNC⁺24]

Table 1: Quantitative comparison on 5 zero-shot affine-invariant depth benchmarks **with author released weights**. We mark the best results in bold and the second best underlined. Discriminative methods are colored in **blue** while generative ones in **green**.

Method	Train Samples	Year	NYUv2 [SHKF12]		KITTI [GLU12]		ETH3D [SSG+17]		ScanNet [DCS+17]		DIODE [VKZ+19]	
			AbsRel ↓	$\delta 1 \uparrow$	AbsRel ↓	$\delta 1 \uparrow$	AbsRel ↓	$\delta 1 \uparrow$	AbsRel ↓	$\delta 1 \uparrow$	AbsRel ↓	$\delta 1 \uparrow$
Metric3Dv2 [HYZ+24]	16M	arXiv'24	3.9	97.9	5.2	97.9	4.0	98.3	2.3	98.9	14.7	89.2
DepthAnything [YKH+24]	63.5M	CVPR'24	<u>4.3</u>	98.0	<u>8.0</u>	<u>94.6</u>	<u>5.8</u>	<u>98.4</u>	<u>4.3</u>	<u>98.1</u>	<u>26.1</u>	75.9
Marigold [KOH+24]	74K	CVPR'24	5.5	96.4	9.9	91.6	6.5	96.0	6.4	95.1	30.8	77.3
GeoWizard [FYH+24]	280K	arXiv'24	5.9	95.9	12.9	85.1	7.7	94.0	6.6	95.3	32.8	75.3
GenPercept [XGL+24]	74K	arXiv'24	6.3	96.0	13.3	84.1	7.2	95.5	6.6	96.0	32.3	76.0
DepthFM [GFP+24]	63K	arXiv'24	8.2	93.2	17.4	71.8	10.1	90.2	9.5	90.3	33.4	72.9

of discriminative models for both depth and surface normal estimation has shown its significance in improving performance, thereby broadening the applications of monocular geometry estimation.

Generative geometry estimation Models. Given the impressive results of recent generative models [RBL+22] in image generation tasks, many studies have endeavored to incorporate generative-based pipelines into geometry estimation. Ji et al. [JCX+23] proposed a method to extend the denoising diffusion process into the modern perception pipeline, which can be generalized to most dense prediction tasks, such as depth estimation. Saxena et al. [SHH+24] formulated optical flow and monocular depth estimation as image-to-image translation using generative diffusion models, without specialized loss functions and model architectures. Zhao et al. [ZRL+23] proposed VPD, a framework that exploits the semantic information of a pre-trained text-to-image diffusion model in visual perception tasks. Ke et al. [KOH+24] introduced a method for affine-invariant monocular depth estimation, where the depth information is derived from retained rich stable diffusion priors. Fu et al. [FYH+24] proposed a foundation model for jointly estimating depth and surface normal from monocular images, which not only achieves surprisingly robust generalization on various types of real or synthetic images but also faithfully captures intricate geometric details. In summary, recent generative-based methods have provided new solutions and demonstrated their applications for depth estimation.

Geometric evaluation metrics. We use widely adopted evaluation metrics for assessing the performance of depth and surface normal estimation. Specifically, for the depth estimation task, we use mean absolute relative error (AbsRel) and accuracy under thresholds ($\delta_i < 1.25^i, i = 1, 2, 3$) for accuracy comparisons. These evaluation metrics for depth estimation are calculated as follows: **(1)** mean absolute relative error (AbsRel): $\frac{1}{n} \sum_{i=1}^n \frac{|z_i - z_i^*|}{z_i^*}$; **(2)** the accuracy under threshold ($\delta_i < 1.25^i, i = 1, 2, 3$): % of z_i s.t. $\max\left(\frac{z_i}{z_i^*}, \frac{z_i^*}{z_i}\right) < 1.25^i$; where z_i is the ground truth depth and z_i^* represents the predicted depth. For surface normal estimation, we calculate the angular error for the pixels with ground truth and report both the median and mean values (lower is better). In addition, we measure the percentage of pixels with an error below $t \in [5.0^\circ, 11.25^\circ, 30.0^\circ]$ (higher is better). Please refer to [BD24] for calculation details.

3 Benchmarking Depth Estimation Foundation Models

3.1 A Brief Overview of SOTA Methods

To demonstrate the performance of the SOTA methods, we consider some latest and representative algorithms, *i.e.*, two discriminative models, (Metric3Dv2 [HYZ+24], Depth-Anything [YKH+24]), and four generative models (Marigold [KOH+24], DepthFM [GFP+24], Geowizard [FYH+24] and GenPercept [XGL+24]). We fairly evaluate their performance by using the official released model weights on 5 popular benchmarks, *i.e.*, NYU v2 [SHKF12], KITTI [GLU12], ETH3D [SSG+17], ScanNet [DCS+17] and DIODE [VKZ+19], in Table 1. Notably, all the methods do not use these benchmarks as training data. We can easily observe that **(1)** Metric3Dv2 [HYZ+24] achieves the best performance on all evaluation datasets, another discriminative-based method, Depth-Anything [YKH+24] achieves the second best performance. Both of them are trained on large-scale datasets, with 16M

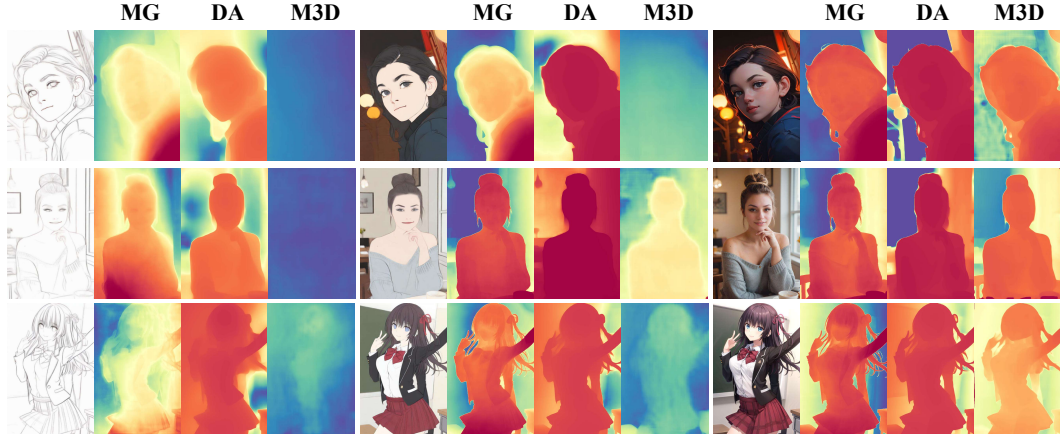


Figure 1: Depth visualization on cartoon images. ‘MG’ indicates Marigold [KOH⁺24], ‘DA’ indicates Depth-Anything [YKH⁺24], ‘M3D’ indicates Metric3Dv2 [HYZ⁺24].

Table 2: Benchmarking depth estimation on Infinigen [RLM⁺23] and BEDLAM [BPTY23] datasets. ‘Standard’ indicates using standard evaluation metrics. ‘Canny’ indicates only evaluating the performance on pixels that belong to canny edges. We mark the best results in bold.

Method	Train Samples	Infinigen-Standard		Infinigen-Canny		BEDLAM-Standard		BEDLAM-Canny	
		AbsRel ↓	$\delta 1$ ↑	AbsRel ↓	$\delta 1$ ↑	AbsRel ↓	$\delta 1$ ↑	AbsRel ↓	$\delta 1$ ↑
Marigold [KOH ⁺ 24]	74K	32.9	80.9	28.0	78.7	16.2	82.4	19.6	80.3
Metric3Dv2 [HYZ ⁺ 24]	16M	14.5	80.7	18.6	77.8	28.1	84.7	26.3	80.8
Depth-Anything [YKH ⁺ 24]	63.5M	12.0	88.4	14.3	84.7	46.2	69.0	46.8	67.8

and 63.5M training data separately. (2) Generative methods can achieve impressive results on these evaluation benchmarks with even a small amount of fine-tuning data.

In addition to quantitative results, we further test their generalization capability by qualitative visualization in several challenging scenes. Fig. 1 demonstrates the results of three algorithms on line drawing images (left), color draft images (middle), and photo-realistic images (right). Surprisingly, Metric3D fails on both line draw images and color draft images, while Marigold [KOH⁺24] and Depth-Anything [YKH⁺24] show some generalization capability on this kind of non-geometrically consistent hand-drawn images. We conjecture that discriminative-based Metric3D does not see cartoon images in the training stage, which leads to poor performance in this scenario. Contrarily, although Marigold [KOH⁺24] also does not see cartoon images in their training set, it leverages the priors stored in the pre-trained Stable Diffusion [RBL⁺22] model. Stable Diffusion [RBL⁺22] model has seen millions of text-cartoon pairs when performing text-to-image generation training. Fig. 2 shows the robustness of existing depth estimation models on challenging scenes like rainy, blurry, dark, and foggy environments. Both Metric3D and Depth-Anything fail on the rainy scene; both Marigold and Metric3D fail to estimate the sky in the second blurry scene. None of the algorithms can handle all environments perfectly. Fig. 3 illustrates the depth estimation results on the Infinigen [RLM⁺23] dataset (first two lines) and BEDLAM [BPTY23] dataset (last line). Infinigen [RLM⁺23] is a photo-realistic rendered dataset with diverse nature scenes. BEDLAM [BPTY23] is a human-centered high-quality rendered dataset with versatile indoor and outdoor scenes. Mainstream depth evaluation metrics overlook the depth accuracy on the edges of the objects. We use these two datasets to demonstrate the fine-grained depth estimation results since both datasets have high-quality annotations. For measuring the accuracy of depth estimation on edges. We use Canny [Can86] edge detector to extract the edge mask from the image and then calculate the traditional depth metrics. As shown in Table 2, Depth-Anything achieves the highest performance on the Infinigen dataset; Marigold achieves the best AbsRel on the BEDLAM [BPTY23] dataset.

In a nutshell, discriminative models trained on large data, *i.e.*, Depth-Anything [YKH⁺24], obtains the highest performance in most cases, while generative models fine-tuned on small data, *e.g.*, Marigold [KOH⁺24], show competitive generalization capability on unseen scenes.

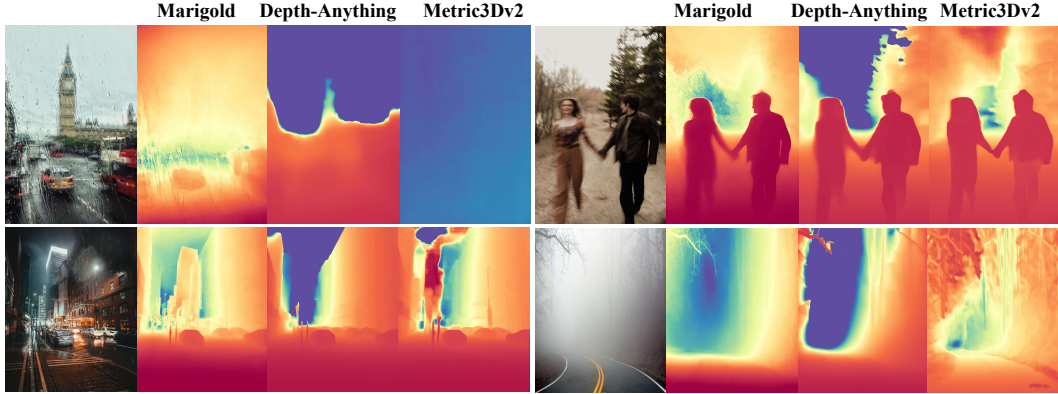


Figure 2: Depth visualization on four challenging scenes, *i.e.*, rainy (top-left), blurry (top-right), dark (bottom-left), and foggy (bottom-right) environments.

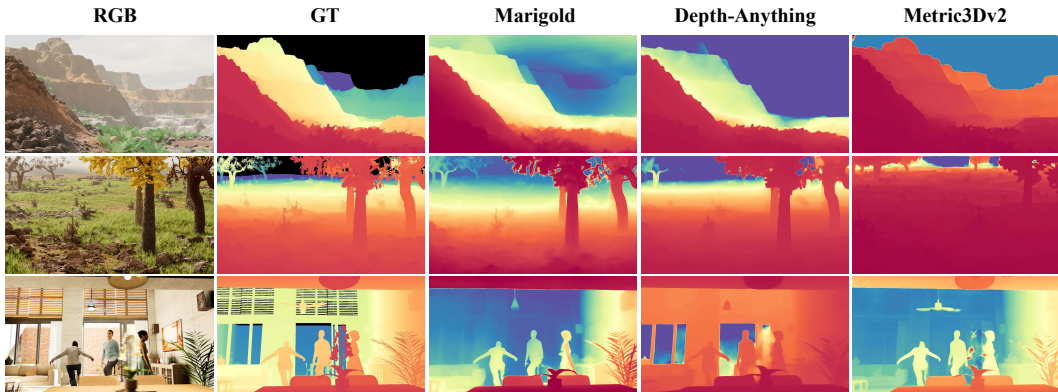


Figure 3: Fine-grained depth estimation comparison. We select two scenes (first two rows) from the Infinigen Dataset [RLM⁺23] and one scene (last row) from the BEDLAM dataset [BPTY23].

3.2 Benchmarking Different Generative Fine-Tuning Paradigms

Several fine-tuning paradigms have been proposed for diffusion-based depth estimation. Based on the network architecture, they can be divided into two categories. The first category of methods (Marigold [KOH⁺24] and DepthFM [GFP⁺24]) concatenate the image latent and depth latent encoded by VAE [KW14] encoder as the input of the UNet latent denoiser. As such, the input channels of the latent denoiser are doubled (8 input channels) to fit the expanded input. The second category methods (DMP [LTLY24] and GenPercept [XGL⁺24]) drop the depth latent, so they follow the original latent denoiser’s architecture (4 input channels). Based on fine-tuning paradigms, they can be divided into four categories. (1) Marigold [KOH⁺24] treats the initial depth latent as standard Gaussian noise and progressively denoise it with the same scheduler as the original Stable Diffusion pipeline. (2) DepthFM also treats the initial depth latent as standard Gaussian noise, however, the difference is that they finetune the denoiser with Flow Matching [LCBH⁺22] pipeline, with auxiliary surface normal loss. (3) DMP [LTLY24] reformulates the task as a blending process, *i.e.*, translating the image latent to depth latent with the Stable Diffusion v-prediction [RBL⁺22] learning target. (4) GenPercept [XGL⁺24] further improve the efficiency of DMP [LTLY24] by proposing a one-step inference pipeline. Based on the amount of fine-tuned parameters, they can be divided into two categories. The first category methods (Marigold, DepthFM, GenPercept) directly fine-tune the UNet parameters. The second category method (DMP) adds LORA [HSW⁺21] layers into the UNet architecture to achieve the goal of depth estimation.

In this section, we fairly benchmark the four fine-tuning protocols by training on the Hypersim dataset (38,387 samples), with 480×640 resolution, 3×10^{-5} learning rate, 96 batch sizes, and 10,000 iterations. We choose Stable Diffusion 2.1 [RBL⁺22] as the base model. As shown in Table 3, (1)

Table 3: Benchmarking different generative finetuning paradigms on 5 zero-shot affine-invariant depth benchmarks. We mark the best results in bold and the second best underlined.

Method	Train Samples	FT Strategies	NYUv2 [SHKF12]		KITTI [GLU12]		ETH3D [SSG ⁺ 17]		ScanNet [DCS ⁺ 17]		DIODE [VKZ ⁺ 19]	
			AbsRel ↓	$\delta 1$ ↑	AbsRel ↓	$\delta 1$ ↑	AbsRel ↓	$\delta 1$ ↑	AbsRel ↓	$\delta 1$ ↑	AbsRel ↓	$\delta 1$ ↑
DMP [LTLY24]	38K	LORA	13.2	85.1	19.2	74.3	16.2	83.7	14.1	84.6	45.6	62.1
DMP [LTLY24]	38K	UNet	10.1	90.6	<u>15.4</u>	<u>80.0</u>	10.0	91.0	10.9	89.0	38.2	68.7
Marigold [KOH ⁺ 24]	38K	UNet	<u>6.9</u>	<u>95.0</u>	13.8	80.7	7.5	93.7	<u>7.1</u>	<u>94.3</u>	28.7	74.6
GenPercept [KOH ⁺ 24]	38K	UNet	6.5	96.1	18.4	69.2	<u>8.5</u>	<u>92.8</u>	6.6	96.4	<u>32.4</u>	<u>74.5</u>
DepthFM [KOH ⁺ 24]	38K	UNet	10.9	89.5	19.2	68.8	12.9	86.3	11.4	87.7	33.6	72.4

Table 4: Inference latency and speed benchmark for different components and methods. ‘Infer Steps’ indicates the minimum repeat times of the U-Net for achieving optimal results. All models are inference with 512×512 resolution, except CLIP [RKH⁺21] (224×224).

Method	Components	Params/M	Macs/GFLOPs	Latency/s	Memory/G	Inference Steps
Depth-Anything [YKH ⁺ 24]	ViT-L [DBK ⁺ 20] + Head	335.3	586.0	0.19	2.24	1
Metric3Dv2 [HYZ ⁺ 24]	ViT-L [DBK ⁺ 20] + Head	411.9	1014.0	0.60	2.67	1
DSINE [BD24]	EfficientNet B5 [TL19] + Head	72.6	38.7	0.06	0.73	1
-	VAE-Tiny [mad23]	2.4	131.9	0.03	0.61	1
-	VAE [KW14]	83.7	1781.2	0.11	0.65	1
Geowizard [FYH ⁺ 24]	CLIP [RKH ⁺ 21]	304.0	77.8	0.04	1.25	1
Marigold-LCM [KOH ⁺ 24]	VAE [KW14] + UNet [RFB15]	949.6	3138.4	0.29	5.27	4
Geowizard [FYH ⁺ 24]	VAE [KW14] + UNet [RFB15] + CLIP [RKH ⁺ 21]	861.2	9846.1	0.85	5.24	10
DepthFM [GFP ⁺ 24]	VAE [KW14] + UNet [RFB15]	949.6	2459.8	0.21	5.40	2
GenPercept [XGL ⁺ 24]	VAE [KW14] + UNet [RFB15]	949.6	2120.4	0.18	5.40	1
GenPercept [XGL ⁺ 24]	VAE-Tiny [mad23] + UNet [RFB15]	868.3	471.1	0.18	5.40	1

Table 5: Benchmarking the inference efficiency of Marigold. We mark the best results in bold.

Method	VAE Version	Infer Steps	NYUv2 [SHKF12]		KITTI [GLU12]		ETH3D [SSG ⁺ 17]		ScanNet [DCS ⁺ 17]		DIODE [VKZ ⁺ 19]	
			AbsRel ↓	$\delta 1$ ↑	AbsRel ↓	$\delta 1$ ↑	AbsRel ↓	$\delta 1$ ↑	AbsRel ↓	$\delta 1$ ↑	AbsRel ↓	$\delta 1$ ↑
Marigold [KOH ⁺ 24]	base	50	5.5	96.4	9.9	91.6	6.5	96.0	6.4	95.1	30.8	77.3
Marigold-LCM [KOH ⁺ 24]	base	4	6.1	95.8	10.1	90.6	6.3	96.0	6.9	94.7	30.9	77.3
Marigold-LCM [KOH ⁺ 24]	tiny [mad23]	4	6.9	95.0	13.8	80.7	7.5	93.7	7.1	94.3	32.8	73.8
Marigold-LCM [KOH ⁺ 24]	tiny [mad23]	1	6.6	95.4	13.0	83.6	7.8	93.2	7.0	94.5	33.3	73.1

Marigold [KOH⁺24] outperforms other protocols in outdoor benchmarks, GenPercept [XGL⁺24] gets the best performance in indoor benchmarks. Overall, Marigold has better generation capability than GenPercept. (2) Fine-tuning all UNet parameters outperforms using LORA layers. (compare line 1 and line 2 on DMP) (3) One-step GenPercept [XGL⁺24] can outperform multi-step DMP [LTLY24]. We conjecture that the RGB blending strategy proposed in DMP makes it hard to decouple image latent and depth latent during the inference stage (see Supp. Mat. for visualization). (4) DepthFM [GFP⁺24] uses flow matching as the fine-tuning protocol for efficient inference (two steps). Although its performance is not comparable with Marigold, we speculate this is due to the gap between the fine-tuning flow pipeline and pre-training v-prediction pipeline in Stable Diffusion 2.1. With the rise of flow-based generative models, *e.g.*, Stable Diffusion 3 [EKB⁺24], it may become a suitable fine-tuning strategy for flow-based models.

3.3 Benchmarking the Inference Efficiency of Depth Estimation Foundation Models

Compared to discriminative models, the inference efficiency may become a bottleneck of the generative-based methods. In this section, we give detailed inference efficiency evaluation in Table 4. We can see that discriminative methods have fewer parameters than generative models. The main inference consumption of the generative models happens on VAE [KW14] and multiple inference steps of UNet. The last line of Table 4 shows that GenPercept [XGL⁺24] can achieve comparable inference latency with Depth-Anything (ViT-Large) and a tiny VAE encoder [mad23]. In Table 5, we found LCM [LTH⁺23] can effectively reduce the inference steps of Marigold [KOH⁺24] while maintaining the performance. Besides, a pre-trained tiny VAE [mad23] can substitute the standard VAE [RBL⁺22] with a minimal performance loss.

Table 6: Benchmarking deterministic and generative depth model with the same training data (77K).

Network	Pretrain Style	Backbone	NYUv2 [SHKF12]		KITTI [GLU12]		ETH3D [SSG ⁺ 17]		ScanNet [DCS ⁺ 17]		DIODE [VKZ ⁺ 19]	
			AbsRel ↓	δ1 ↑	AbsRel ↓	δ1 ↑	AbsRel ↓	δ1 ↑	AbsRel ↓	δ1 ↑	AbsRel ↓	δ1 ↑
ViT+DPT Head	Random init	ViT-L	21.1	62.5	27.2	53.1	23.4	61.1	19.2	67.4	32.4	57.7
ViT+DPT Head	DINOv2 [ODM ⁺ 24]	ViT-L	4.9	97.5	8.5	94.1	8.1	97.0	5.1	97.6	24.5	74.6
Marigold [KOH ⁺ 24]	SD21 [RBL ⁺ 22]	UNet	6.9	95.8	12.2	85.7	9.2	95.5	7.1	95.4	25.2	73.0
Marigold [KOH ⁺ 24]	SDXL [PEL ⁺ 23]	UNet	6.8	95.8	11.1	89.2	8.9	96.7	6.3	96.2	24.5	73.6

Table 7: Benchmarking depth estimation foundation models on more diverse benchmarks. We mark the best results in bold.

Network	Pretrain Style	Backbone	Train Samples	InspaceType [WGH ⁺ 23]		MatrixCity [LJX ⁺ 23]		Infinigen [RLM ⁺ 23]	
				AbsRel ↓	δ1 ↑	AbsRel ↓	δ1 ↑	AbsRel ↓	δ1 ↑
Metric3Dv2 [HYZ ⁺ 24]	DINOv2 [ODM ⁺ 24]	ViT-L	16M	10.1	89.7	9.5	89.3	14.5	80.7
Depth-Anything [YKH ⁺ 24]	DINOv2 [ODM ⁺ 24]	ViT-L	63.5M	8.2	92.9	16.4	89.7	12.0	88.4
ViT+DPT Head	DINOv2 [ODM ⁺ 24]	ViT-L	77K	8.4	94.0	28.0	82.4	11.4	89.5
Marigold [KOH ⁺ 24]	SD21 [RBL ⁺ 22]	UNet	77K	9.2	92.7	17.0	82.9	14.1	83.9

3.4 Benchmarking Discriminative and Generative Models on the Same Training Data

Can discriminative depth estimation models achieve competitive results with small-scale high-quality training datasets like generative-based methods? To answer this question, we benchmark discriminative and generative geometry model with the same amount of training data and the same training strategy. Specifically, we use three training datasets, *i.e.*, Hypersim (38,387) [RRR⁺21], Virtual Kitti (16,790) [GWCV16] and Tartanair (31,008) [WZW⁺20], with total 77,897 samples. Both models are trained with 20,000 iterations, with a total batch size of 96 on 4 GPUs. For the discriminative depth model, we follow the network architecture of Depth-Anything [YKH⁺24] (ViT-Large backbone pre-trained with DINOv2 and DPT [RBK21] head), supervised with the affine-invariant loss [YKH⁺24]. For the generative geometry model, we choose Marigold [KOH⁺24] as our baseline.

We can see from Table 6 that (1) the discriminative model is largely inferior to generative-based Marigold on all evaluation datasets without DINOv2 pre-train (line 1 *vs.* line 3). However, the discriminative model beats Marigold by a large margin when initialized with DINOv2 pre-train weight (line 2 *vs.* line 3); (2) scale-up Marigold from SD21 to SDXL brings consistent improvement in all benchmarks. We can see from Table 7 that our discriminative model trained on 77K data outperforms Metric3Dv2 [HYZ⁺24] in all three datasets, and, is comparable with Depth-Anything [YKH⁺24] on two datasets (InspaceType and Infinigen). This phenomenon suggests that **high-quality fine-tuning data**, rather than large-scale training data, is indispensable for discriminative models to achieve strong generalizable performance. *The qualitative visualization of discriminative models is not as good as generative models, more visualizations are available in the Supp. Mat.*

4 Benchmarking Surface Normal Estimation Foundation Models

4.1 A Brief Overview of SOTA Methods

DSINE [BD24] and Metric3Dv2 [HYZ⁺24] are two representative discriminative surface estimation models, which leverage the geometry priors from two distinct perspectives. DSINE leverages two forms of inductive bias: (1) per-pixel ray direction, and (2) the relationship between the neighboring surface normal, to learn a generalizable surface normal estimator. Metric3Dv2 [HYZ⁺24] proposes to optimize the surface normal map by distilling diverse data knowledge from the estimated metric depth. Different from discriminative models, GeoWizard [FYH⁺24] is a generative surface normal estimator without using any inductive bias from the geometry priors. It purely relies on pre-trained diffusion priors to estimate the surface normal map. Table 9 summarizes their performance on six benchmarks. The Mushroom [RWC⁺24] (indoor), T&T [KPZK17] (outdoor), and Infinigen [RLM⁺23] (wild) datasets are constructed by us to add more diverse scenes with accurate surface normal labels in the evaluation benchmarks. We can see that Metric3Dv2 [HYZ⁺24] outperform DSINE [BD24] and GeoWizard [FYH⁺24] in most datasets. Note it is an unfair comparison since (1) Metric3Dv2 [HYZ⁺24] is trained on 16M images, while DSINE is trained on 160K images,

Table 8: Quantitative evaluation of the generalization capabilities possessed by **various methods with official released weights**. For each metric, the best results are bolded. Discriminative methods are colored in **blue** while generative ones in **green**.

Method	NYU v2 [SHKF12]						ScanNet [DCS ⁺ 17]						Sintel [BWSB12]								
	mean	med	5.0°	7.5°	11.25°	22.5°	30°	mean	med	5.0°	7.5°	11.25°	22.5°	30°	mean	med	5.0°	7.5°	11.25°	22.5°	30°
Metric3Dv2 [HYZ ⁺ 24]	13.5	6.7	40.1	53.5	65.9	82.6	87.7	11.8	5.5	46.6	60.7	71.6	85.4	89.7	22.8	14.2	18.4	28.5	41.6	66.7	75.8
DINSE [BD24]	16.4	8.4	32.8	46.3	59.6	77.7	83.5	18.3	9.3	27.1	42.0	56.3	75.0	81.2	32.0	23.9	9.0	15.0	23.8	47.5	59.4
Geowizard [FYH ⁺ 24]	19.8	11.2	18.0	32.7	50.2	73.0	79.9	21.1	11.9	15.9	29.7	47.4	70.7	77.8	36.1	28.4	4.1	8.6	16.9	39.8	52.5
Method	MuSHRoom Subset [RWC ⁺ 24] (Indoor)						T&T Subset [KPZK17] (Outdoor)						Infinigen Subset [RLM ⁺ 23] (Wild)								
	mean	med	5.0°	7.5°	11.25°	22.5°	30°	mean	med	5.0°	7.5°	11.25°	22.5°	30°	mean	med	5.0°	7.5°	11.25°	22.5°	30°
Metric3Dv2 [HYZ ⁺ 24]	14.3	7.9	31.9	48.1	61.8	81.7	87.2	22.3	14.1	19.2	31.4	43.0	64.8	73.5	32.6	27.3	5.1	10.1	17.8	41.3	54.4
DINSE [BD24]	14.8	8.6	28.1	44.6	59.7	80.4	87.0	17.3	11.0	24.2	37.3	50.6	74.1	82.4	35.9	32.6	2.1	4.6	9.8	30.5	45.1
Geowizard [FYH ⁺ 24]	16.5	10.7	14.7	30.5	52.5	79.6	86.2	20.8	13.4	10.7	23.4	42.2	70.3	78.5	36.2	32.0	1.8	4.0	8.86	30.8	46.2

and GeoWizard is trained on 280K images. (2) DSINE use a much smaller backbone, EfficientNet-B5 [TL19], while Metric3Dv2 [HYZ⁺24] employs the ViT-Large [DBK⁺20] backbone, pretrained using DINOv2 with registers [DOMB23].

4.2 Benchmarking Discriminative and Generative Models on the Same Training Data

In this section, we fairly benchmark discriminative DSINE [BD24] and several representative generative geometry models, *i.e.*, Marigold [KOH⁺24], DMP [LTLY24], GenPercept [XGL⁺24], and DepthFM [GFP⁺24], with 5 training datasets, Hypersim [RRR⁺21] (38, 387), Tartanair [WZW⁺20] (31, 008), Virtual Kitti [GWCV16] (16, 790), BlendedMVS [YLL⁺20] (17, 819), ClearGrasp [SMP⁺20] (22, 720), a total of 126, 724 samples. For generative-based models, we represent the output surface normals as unit vectors. We follow DSINE [BD24] to represent the outputs of discriminative-based model as axis-angles with three degrees of freedom. All models are trained with 20, 000 iterations, 96 batch sizes, 480×640 resolution on 4 A800 GPUs. All generative-based models use 3×10^{-5} learning rate. For discriminative model, we follow DSINE [BD24] to use 3×10^{-5} learning rate for the backbone and 3×10^{-4} learning rate for the decoder.

We can see from Table 8 that (1) DSINE can scale up the performance by using ViT-Large backbone with DINOv2 pretrain (compared with ImageNet pretrained Efficient-B5 backbone). (2) For generative-based fine-tuning protocols, DepthFM [GFP⁺24] outperforms other paradigms in most benchmarks. We attribute this to the decoder supervision during the training. Paradigms that requires multi-step denoising inference steps, *e.g.*, Marigold [KOH⁺24] and DMP [LTLY24] are not suitable to perform decoder supervision during the training. (3) Discriminative models, equipped with inductive bias, outperform generative-based models with only diffusion priors. It is promising to inject inductive bias into the diffusion-based models, as such, the surface normal estimator can effectively leverage the diffusion priors and inductive bias to boost the performance. (4) DSINE (ViT-Large in Table 8) trained with 120K samples achieves comparable performance with Metric3Dv2 trained with 16M samples (Table 9). The results verify the point that data-quality is more important than the data-scale.

5 Benchmarking Geometric Correspondence

Can current monocular geometry estimation models improve the 3D awareness of the original representation models, e.g., DINOv2 and Stable Diffusion? To answer the question, we follow Probe3D [BRM⁺24] by using geometric correspondence estimation, since 3D awareness implies consistency of representations across different views. Specifically, given two views of the same scene, geometric correspondence estimation needs to identify pixels across views that depict the same point in 3D space. We extract feature maps from either trained monocular geometry models or representation models, *e.g.*, DINOv2, and directly compute correspondence between the dense feature maps of different views. We use Paired ScanNet [DCS⁺17] for scene evaluation and NAVI wild set [JME⁺24] for object evaluation. Following [BRM⁺24], we report the correspondence recall, *i.e.*, the percentage of correspondence that falls within some defined distance. We can see from Fig. 4 that:

Table 9: Quantitative evaluation of the generalization capabilities **with the same training data** on different benchmarks. The best results are bolded. ‘EB5’ indicates ImageNet [DDS⁺09] pre-trained EfficientNet-B5 [TL19]. ‘ViT-L’ indicates DINOv2 [ODM⁺24] pre-trained ViT-Large. The best results are **bolded**. The best results of generative-based models are underlined.

Method	Backbone	NYUv2 [SHKF12]						ScanNet [DCS ⁺ 17]						Sintel [BWSB12]								
		mean	med	5.0°	7.5°	11.25°	22.5°	30°	mean	med	5.0°	7.5°	11.25°	22.5°	30°	mean	med	5.0°	7.5°	11.25°	22.5°	30°
DSINE [BD24]	EB5 [TL19]	19.2	10.0	27.1	40.1	53.9	73.8	80.1	17.3	11.0	24.2	37.3	50.6	74.1	82.4	35.9	32.6	2.1	4.6	9.8	30.5	45.1
DSINE [BD24]	ViT-L [ODM ⁺ 24]	16.2	8.2	32.8	46.9	60.6	78.5	84.1	16.1	7.4	34.5	50.6	63.8	79.4	84.3	24.6	16.1	11.1	21.1	35.1	63.8	74.1
GenPercept [XGL ⁺ 24]	UNet [RFB15]	<u>17.8</u>	<u>9.5</u>	24.1	40.5	55.9	75.7	82.2	<u>18.5</u>	<u>9.4</u>	23.0	40.2	56.7	75.4	<u>81.3</u>	38.6	27.1	4.5	9.1	18.0	42.5	54.2
Marigold [KOH ⁺ 24]	UNet [RFB15]	20.2	10.9	21.8	36.0	51.2	72.8	79.4	20.5	10.3	19.7	36.0	53.5	73.6	79.2	41.3	28.7	5.5	11.1	19.7	40.9	51.7
DMP [LTLY24]	UNet [RFB15]	21.9	11.3	19.7	34.2	49.7	71.1	77.6	22.5	11.2	17.6	32.5	50.3	71.2	76.9	45.0	39.3	4.2	7.9	13.8	29.9	39.0
DepthFM [GFP ⁺ 24]	UNet [RFB15]	<u>17.8</u>	<u>9.3</u>	<u>27.7</u>	<u>41.9</u>	<u>56.5</u>	<u>76.7</u>	<u>82.5</u>	<u>18.5</u>	<u>8.6</u>	<u>28.4</u>	<u>44.7</u>	<u>58.8</u>	<u>75.6</u>	<u>81.0</u>	<u>34.1</u>	<u>25.8</u>	<u>7.1</u>	<u>13.5</u>	<u>22.0</u>	<u>44.8</u>	<u>55.7</u>

Method	Backbone	MuSHRoom Subset [RWC ⁺ 24] (Indoor)						T&T Subset [KPZK17] (Outdoor)						Infinitgen Subset [RLM ⁺ 23] (Wild)								
		mean	med	5.0°	7.5°	11.25°	22.5°	30°	mean	med	5.0°	7.5°	11.25°	22.5°	30°	mean	med	5.0°	7.5°	11.25°	22.5°	30°
DSINE [BD24]	EB5 [TL19]	17.9	10.1	23.9	38.9	53.8	75.8	82.5	21.7	15.4	13.4	25.7	39.0	64.4	75.2	36.5	32.7	2.0	4.4	9.3	29.8	44.8
DSINE [BD24]	ViT-L [ODM ⁺ 24]	12.8	6.9	34.6	53.5	67.9	84.9	89.6	18.8	11.2	22.5	36.3	49.9	71.1	79.5	33.6	28.7	2.7	5.9	13.1	38.3	52.2
GenPercept [XGL ⁺ 24]	UNet [RFB15]	<u>15.0</u>	<u>7.9</u>	<u>32.4</u>	<u>48.0</u>	<u>62.7</u>	<u>80.6</u>	<u>86.3</u>	27.4	14.0	17.8	30.1	43.1	63.7	71.0	38.8	33.5	2.1	4.9	10.5	31.2	44.3
Marigold [KOH ⁺ 24]	UNet [RFB15]	17.7	9.9	19.6	36.8	55.7	77.0	83.1	29.1	14.6	14.4	26.0	40.3	63.0	70.2	39.2	34.0	2.4	5.4	11.5	31.4	43.9
DMP [LTLY24]	UNet [RFB15]	20.4	10.0	19.3	36.0	55.2	73.8	79.1	27.7	17.9	9.1	17.2	31.9	57.9	66.1	43.1	38.1	1.7	4.0	9.5	26.3	38.1
DepthFM [GFP ⁺ 24]	UNet [RFB15]	17.0	9.0	25.9	42.5	58.9	77.4	82.4	<u>22.1</u>	<u>13.9</u>	<u>14.2</u>	<u>26.7</u>	<u>42.1</u>	<u>65.4</u>	<u>74.1</u>	<u>31.9</u>	<u>27.9</u>	<u>2.5</u>	<u>5.4</u>	<u>11.6</u>	<u>38.3</u>	<u>54.0</u>

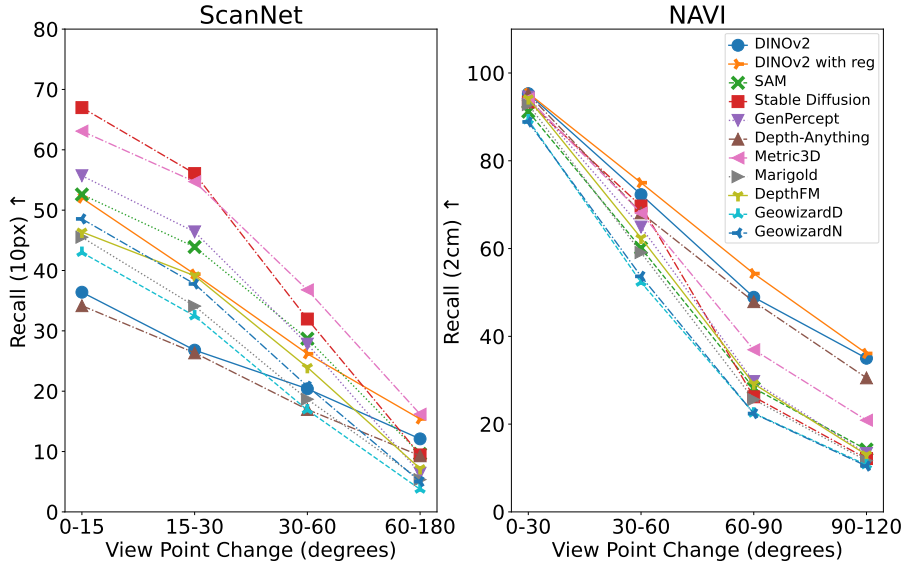


Figure 4: Geometry correspondences evaluation. ‘GeowizardD’, ‘GeowizardN’ indicate depth and normal features from Geowizard.

1. Depth-Anything, pretrained with DINOv2 [ODM⁺24] and fine-tuned on 77K training samples, is comparable to the original DINOv2; Metric3Dv2 pretrained with DINOv2-reg [DOMB23] outperforms original DINOv2-reg on ScanNet and inferior to original DINOv2-reg on NAVI dataset. While generative-based models, *i.e.*, Marigold, DepthFM, GenPercept, and Geowizard, are inferior to the original Stable Diffusion [RBL⁺22] model on both datasets.
2. All models struggle with larger view changes, while generative-based models see a larger drop. In general, monocular geometry estimation models are not 3D-consistent with large viewpoints and thus not yet good enough to encode the 3D structure of the real-world scenario.

6 Conclusion and Discussion

In this work, we present the *first* large-scale benchmarking of discriminative and generative geometry estimation foundation models with diverse evaluation datasets. We identify that with a strong pre-train model, either Stable Diffusion or DINOv2, the fine-tuning data quality is a more important factor than fine-tuning data scale and model architecture to achieve generalizable geometry estimation. We believe that this benchmarking study can provide strong baselines for unbiased comparisons in geometry estimation studies. Limitations and future works are discussed in the Supp. Mat.

A Appendix

Benchmarking: We introduce new benchmarks with diverse scenes and high-quality annotations to overcome limitations in scene diversity and label quality of existing benchmarks.

Findings: The study reveals that discriminative models pre-trained on large data can outperform generative models with less but high-quality synthetic data, suggesting the importance of data quality over quantity and architecture.

A.1 Depth Estimation Visualization of Different Methods

We visualize the depth estimation results in Fig. 5 and Fig. 6.

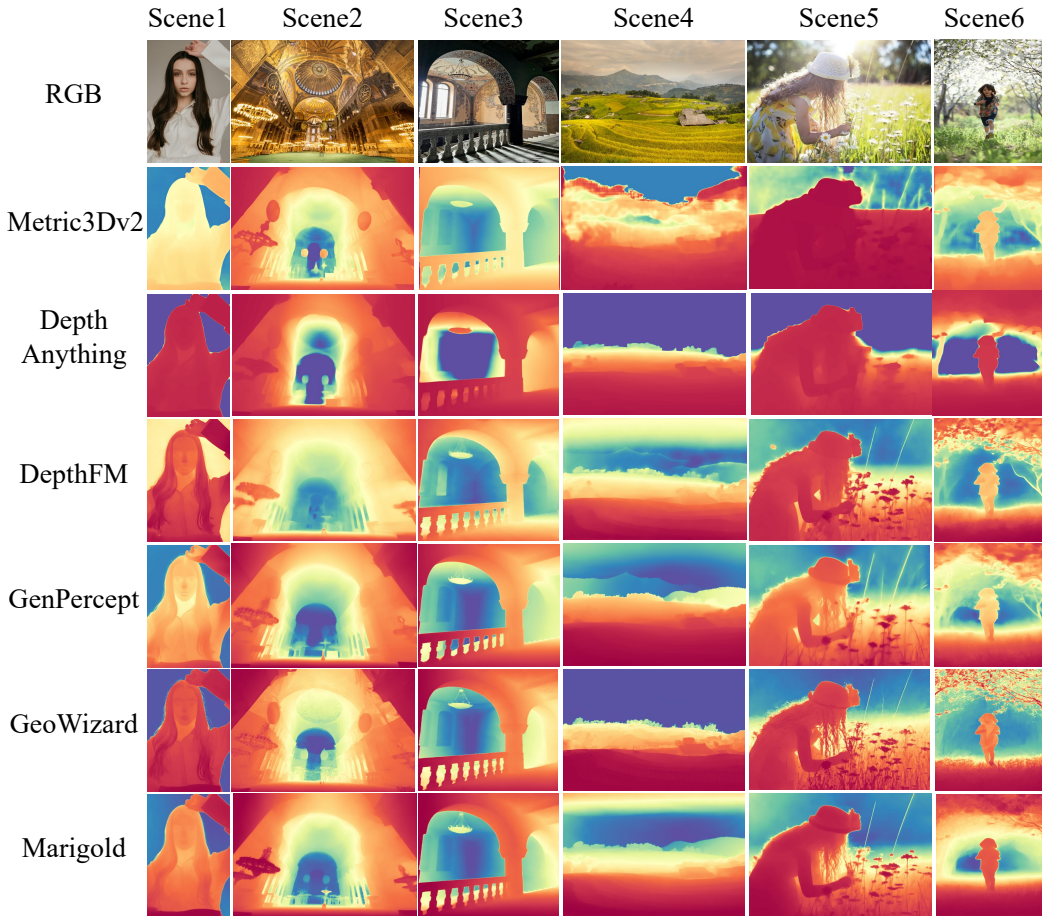


Figure 5: Visualization of different depth estimation methods.

A.2 Surface Normal Estimation Visualization of Different Methods

We visualize the surface normal estimation results in Fig. 7 and Fig. 8.

A.3 Correspondence Estimation Results

We give more detailed correspondence estimation results in Table 10 for reference. Note that we find that multi-step inference, *e.g.*, 10 steps, can improve the performance of Stable Diffusion in correspondence estimation tasks. Metric3Dv2 [HYZ⁺24] employs DINOv2 with registers [DOMB23] as the backbone, which has higher performance than DINOv2 without registers [ODM⁺24].

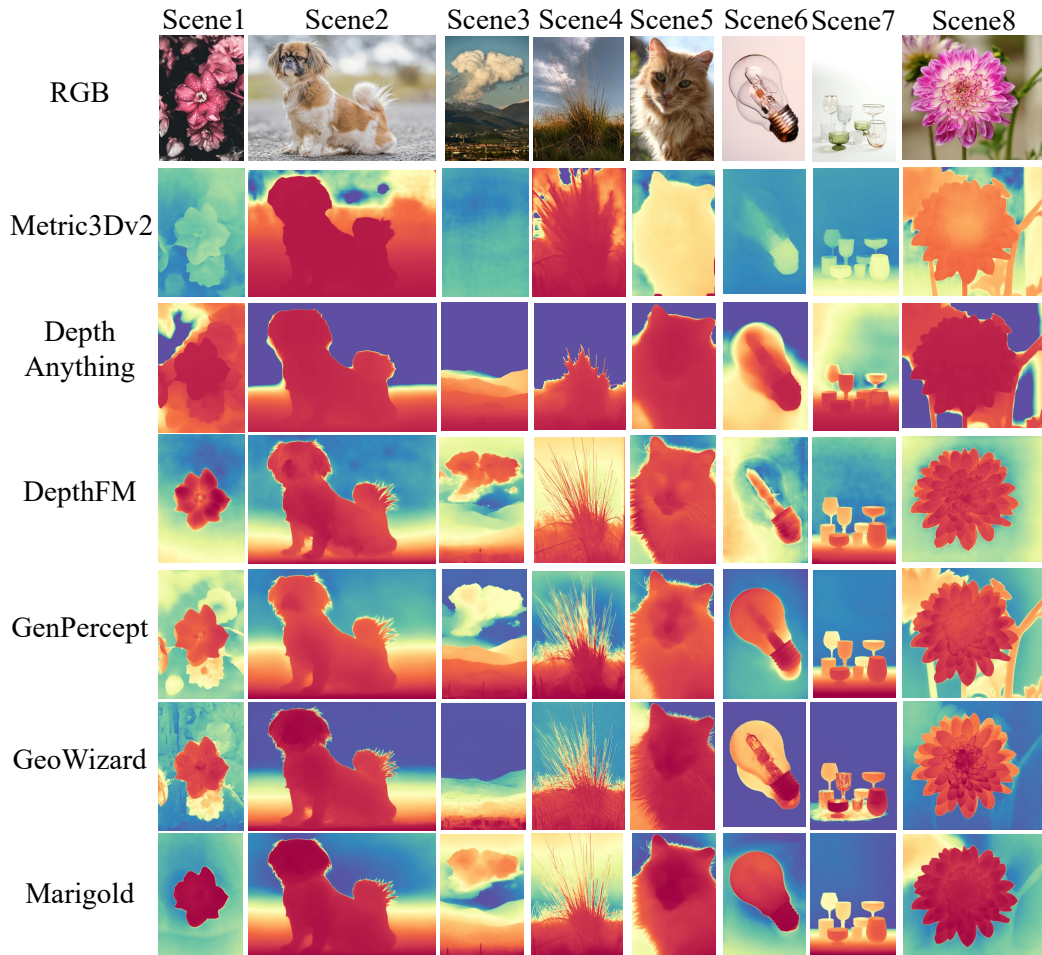


Figure 6: Visualization of different depth estimation methods.

A.4 Surface Normal Estimation Datasets

NYUv2 [SHKF12] is an real indoor dataset comprised RGB-D video sequences from a variety of indoor scenes captured from the Microsoft Kinect. We evaluate on the official test (654 images) set with the ground-truth surface normal generated by Ladicky *et al.* [LZP14].

ScanNet [DCS⁺17] is a real RGB-D video dataset of indoor scenes. We use the ground-truth surface normal and test split (800 sampled images) provided by FrameNet [HZFG19]. To mitigate the noise, it first computes two (X and Y) tangent principal directions by adopting the 4-RoS field using QuadriFlow [HZN⁺18] as proposed by TextureNet [HZY⁺19], and the ground-truth normal can be directly computed as the cross product of them.

DIODE [VKZ⁺19] 1024×768 collects both outdoor and indoor scenes. It collects high-quality data, but it contains very low diversity with only 2 scenes for evaluation.

Sintel [BWSB12] is a synthetic dataset derived from an open-source 3D animated short film. We calculate the ground-truth surface normal with the provided ground-truth depth maps and intrinsic parameters following the depth-to-normal procedure of DSINE [BD24].

BEDLAM [BPTY23] contains synthetic monocular RGB videos with ground-truth 3D bodies with varying numbers of people in realistic scenes with varied lighting and camera motions. We calculate the ground-truth surface normal with the provided ground-truth depth maps and intrinsic parameters following the depth-to-normal procedure of DSINE [BD24].

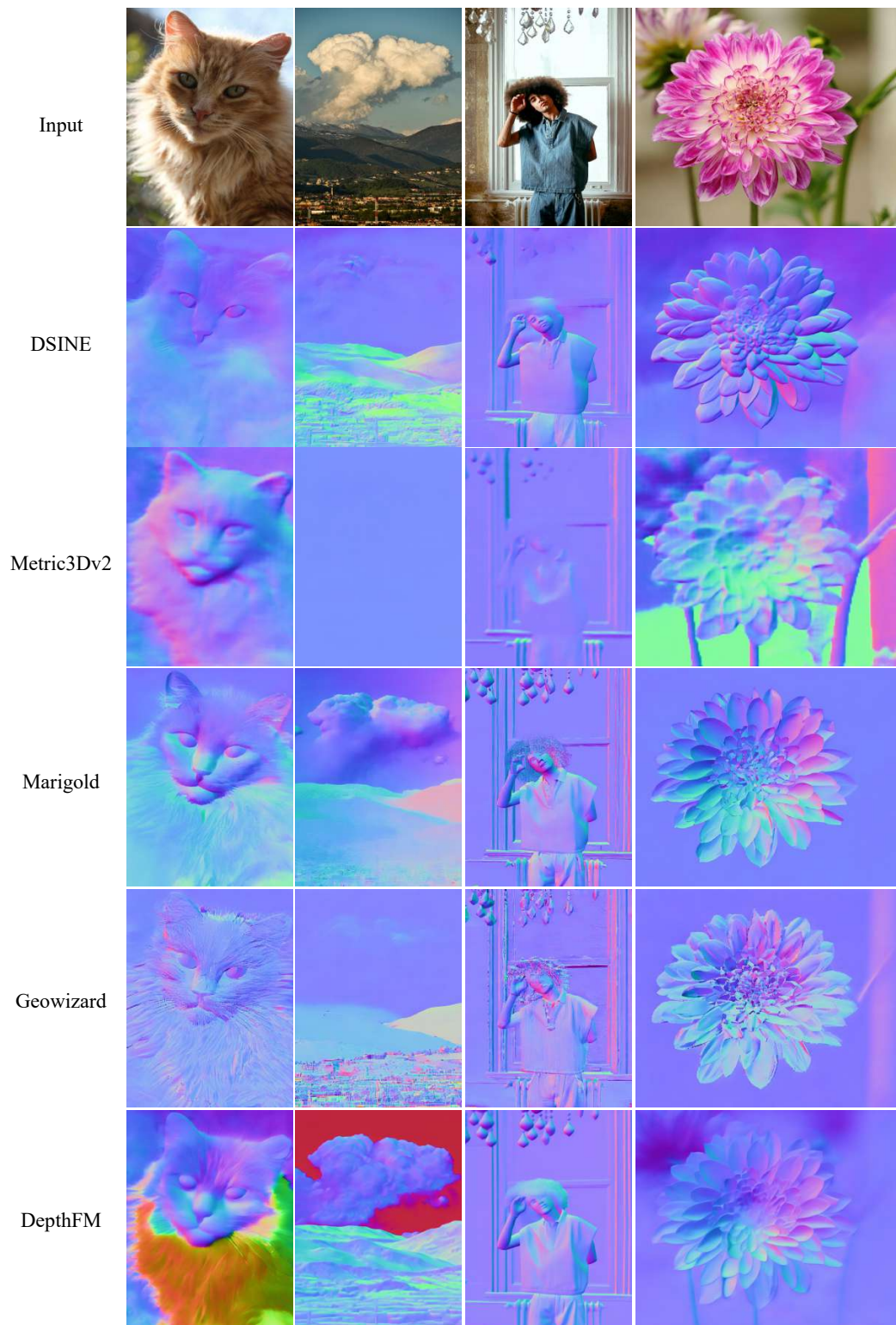


Figure 7: Visualization of different surface normal estimation methods.

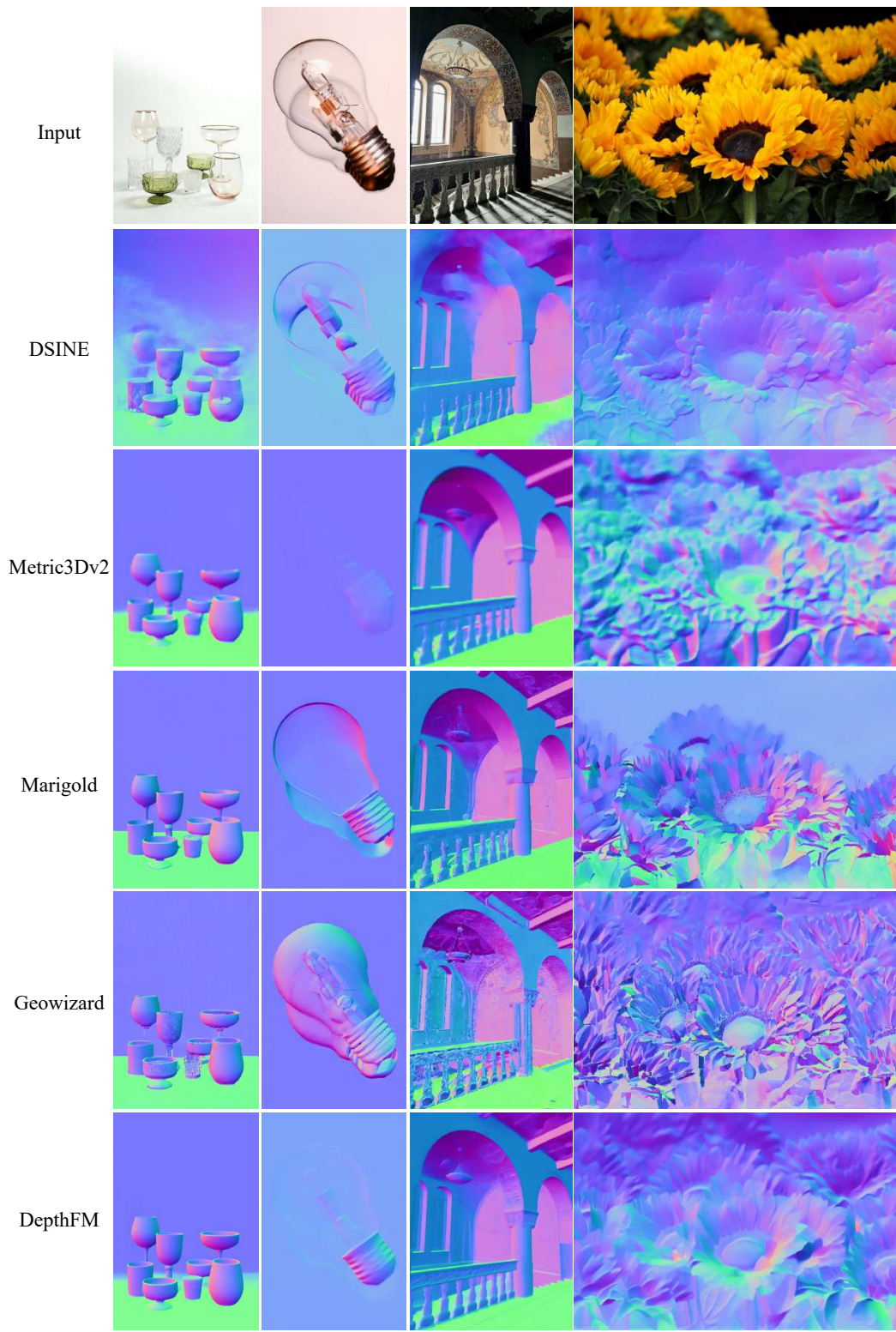


Figure 8: Visualization of different surface normal estimation methods.

Table 10: **Correspondence Estimation Results.** The results are presented for features extracted at different layers with performance binned based on the viewpoint variation for the image pair. ‘DA’ indicates Depth-Anything. ‘DA (77K)’ indicates Depth-Anything trained with only 77K synthetic data. ‘SD10’ indicates Stable Diffusion model inference 10 steps. ‘MIX’ indicates using a mixture of datasets during the training. The higher the recall in the table, the better the performance.

Model	Architecture	Dataset	Layers	Spair-71k				Paired ScanNet				NAVI			
				$d=0$	$d=1$	$d=2$	all	θ_0^{15}	θ_{15}^{30}	θ_{30}^{60}	θ_{60}^{180}	θ_0^{30}	θ_{30}^{60}	θ_{60}^{90}	θ_{90}^{120}
Pre-train Models															
DINOV2 [ODM ⁺ 24]	ViT-L14	LVD	Block0	8.5	6.2	5.3	7.5	17.2	14.1	10.1	4.7	66.2	37.2	19.6	11.5
DINOV2 [ODM ⁺ 24]	ViT-L14	LVD	Block1	25.0	14.0	10.8	19.3	29.0	20.8	13.5	5.2	92.1	57.9	25.6	12.8
DINOV2 [ODM ⁺ 24]	ViT-L14	LVD	Block2	53.9	34.6	31.6	44.5	35.2	24.1	16.3	6.6	95.3	70.0	35.4	18.5
DINOV2 [ODM ⁺ 24]	ViT-L14	LVD	Block3	62.8	53.3	54.2	57.2	36.5	27.0	20.8	12.2	92.2	72.3	48.9	35.0
DINOV2 [DOMB23]	ViT-L14+reg	LVD	Block0	12.2	8.8	8.1	10.4	14.0	14.2	11.4	5.0	79.9	40.8	24.5	13.6
DINOV2 [DOMB23]	ViT-L14+reg	LVD	Block1	41.2	22.8	17.1	32.0	52.0	39.4	23.7	9.1	95.4	65.6	32.7	15.8
DINOV2 [DOMB23]	ViT-L14+reg	LVD	Block2	64.2	45.9	42.4	55.0	50.6	39.3	26.2	12.0	95.2	75.0	49.1	28.6
DINOV2 [DOMB23]	ViT-L14+reg	LVD	Block3	59.3	53.2	54.9	55.0	45.0	35.4	26.1	15.4	88.6	71.2	54.3	36.1
SAM [KMR ⁺ 23]	ViT-L16	SA-1B	Block0	9.9	6.1	5.4	8.0	14.5	9.9	7.5	3.5	78.0	43.3	20.4	11.4
SAM [KMR ⁺ 23]	ViT-L16	SA-1B	Block1	22.6	15.8	12.5	18.3	37.2	29.7	19.7	6.2	86.4	52.0	23.8	12.5
SAM [KMR ⁺ 23]	ViT-L16	SA-1B	Block2	34.8	23.1	17.0	28.2	47.6	40.4	27.3	8.7	91.2	60.1	28.2	14.2
SAM [KMR ⁺ 23]	ViT-L16	SA-1B	Block3	30.2	18.1	13.0	24.1	52.6	43.9	28.7	9.6	88.5	57.6	26.9	13.5
SD10 [RBL ⁺ 22]	UNet	LAION	Block0	13.2	5.3	3.5	9.2	10.8	5.4	3.2	1.3	75.1	32.5	16.6	7.4
SD10 [RBL ⁺ 22]	UNet	LAION	Block1	58.6	36.4	28.6	47.8	67.0	56.1	32.0	8.7	93.4	59.7	26.2	11.4
SD10 [RBL ⁺ 22]	UNet	LAION	Block2	24.0	16.8	13.4	20.2	61.4	49.5	28.4	9.4	79.0	42.5	22.3	12.2
SD10 [RBL ⁺ 22]	UNet	LAION	Block3	4.6	4.3	4.4	4.3	17.2	12.8	8.9	5.0	35.3	22.9	15.2	11.0
Deterministic Geometry Foundation Models															
MiDaS [RBK21]	ViT-L16	MIX 6	Block0	15.6	10.2	8.7	13.0	50.3	39.0	24.4	11.2	79.0	49.1	25.0	14.5
MiDaS [RBK21]	ViT-L16	MIX 6	Block1	27.3	22.8	23.2	24.5	56.4	47.4	31.6	13.9	83.2	56.0	32.1	21.6
MiDaS [RBK21]	ViT-L16	MIX 6	Block2	28.2	23.4	25.1	25.5	55.5	46.0	30.8	14.3	82.2	56.3	33.1	22.9
MiDaS [RBK21]	ViT-L16	MIX 6	Block3	25.8	21.3	23.6	23.4	52.4	42.1	27.6	13.1	79.6	53.0	31.4	21.6
DA [YKH ⁺ 24]	ViT-L16	MIX	Block0	8.0	6.1	5.3	6.8	21.4	17.5	12.2	5.4	66.1	35.6	20.6	12.5
DA [YKH ⁺ 24]	ViT-L16	MIX	Block1	24.4	13.8	11.1	19.4	34.2	26.4	17.0	6.1	92.4	55.9	27.7	14.0
DA [YKH ⁺ 24]	ViT-L16	MIX	Block2	51.4	31.6	28.4	42.2	30.2	23.5	16.2	6.8	95.2	68.1	35.1	17.5
DA [YKH ⁺ 24]	ViT-L16	MIX	Block3	58.9	48.6	49.7	53.5	29.8	21.4	16.8	9.3	90.9	67.8	47.9	30.5
DA(77K) [YKH ⁺ 24]	ViT-L16	MIX	Block0	8.0	5.8	5.2	6.7	18.3	15.1	10.7	5.0	63.6	34.9	20.4	12.4
DA(77K) [YKH ⁺ 24]	ViT-L16	MIX	Block1	24.2	13.6	11.0	19.1	34.4	25.7	16.6	6.4	92.4	54.6	26.9	13.7
DA(77K) [YKH ⁺ 24]	ViT-L16	MIX	Block2	50.8	31.0	28.0	41.6	43.4	32.9	23.2	8.9	94.9	67.0	34.9	17.8
DA(77K) [YKH ⁺ 24]	ViT-L16	MIX	Block3	53.6	42.2	43.4	47.7	38.4	29.8	21.7	11.8	92.8	71.9	50.7	31.0
Metric3Dv2 [HYZ ⁺ 24]	ViT-L16	MIX	Block0	12.0	8.6	7.9	10.1	10.2	10.5	8.7	4.3	79.1	39.7	23.5	12.7
Metric3Dv2 [HYZ ⁺ 24]	ViT-L16	MIX	Block1	39.0	22.0	16.0	30.7	55.7	42.8	25.2	8.8	94.2	61.4	29.6	14.2
Metric3Dv2 [HYZ ⁺ 24]	ViT-L16	MIX	Block2	60.2	41.5	39.8	51.6	63.1	54.7	36.8	14.8	94.1	68.1	36.9	20.9
Metric3Dv2 [HYZ ⁺ 24]	ViT-L16	MIX	Block3	53.6	42.3	42.8	48.0	59.5	50.3	35.1	16.3	86.6	56.5	29.6	17.2
Generative Geometry Foundation Models															
Marigold [KOH ⁺ 24]	UNet	MIX	Block0	14.0	4.6	3.5	9.6	8.4	5.8	3.4	1.3	81.7	37.0	17.0	8.0
Marigold [KOH ⁺ 24]	UNet	MIX	Block1	53.8	29.5	23.7	42.5	42.2	32.4	18.7	4.4	92.8	59.1	25.6	11.7
Marigold [KOH ⁺ 24]	UNet	MIX	Block2	27.2	15.8	12.5	21.3	45.5	34.1	18.1	5.4	83.5	45.4	21.5	11.2
Marigold [KOH ⁺ 24]	UNet	MIX	Block3	8.0	6.4	6.3	7.1	18.0	12.8	7.5	3.5	43.3	25.2	15.9	9.8
DepthFM [GFP ⁺ 24]	UNet	MIX	Block0	20.0	8.4	6.1	14.3	23.1	16.4	7.4	2.2	85.9	40.6	17.0	8.0
DepthFM [GFP ⁺ 24]	UNet	MIX	Block1	50.8	31.4	25.2	42.1	46.4	39.1	24.0	7.2	94.1	62.4	29.2	13.0
DepthFM [GFP ⁺ 24]	UNet	MIX	Block2	22.6	13.8	10.7	18.8	46.0	36.7	20.0	6.2	80.5	41.7	20.7	11.0
DepthFM [GFP ⁺ 24]	UNet	MIX	Block3	3.9	3.5	3.0	3.6	11.2	8.4	6.3	3.8	39.0	25.6	16.3	10.4
GeowizardD [FYH ⁺ 24]	UNet	MIX	Block0	13.7	4.7	2.9	9.7	8.0	5.1	3.2	1.34	81.9	35.1	16.6	8.5
GeowizardD [FYH ⁺ 24]	UNet	MIX	Block1	41.3	19.1	13.4	31.2	43.0	32.5	16.9	3.8	89.3	52.3	22.5	10.7
GeowizardD [FYH ⁺ 24]	UNet	MIX	Block2	20.2	11.4	8.4	16.3	38.3	27.1	12.8	3.7	71.1	35.4	17.8	10.1
GeowizardD [FYH ⁺ 24]	UNet	MIX	Block3	8.5	5.7	5.8	7.2	13.8	9.9	5.4	2.7	32.5	20.1	12.7	8.1
GeowizardN [FYH ⁺ 24]	UNet	MIX	Block0	11.1	3.6	2.9	7.6	8.5	5.1	3.0	1.3	80.6	33.9	15.1	7.6
GeowizardN [FYH ⁺ 24]	UNet	MIX	Block1	43.3	20.2	15.5	32.8	48.6	37.8	20.8	5.0	88.8	53.7	22.4	10.4
GeowizardN [FYH ⁺ 24]	UNet	MIX	Block2	22.5	12.3	9.4	18.0	43.4	32.8	16.3	4.5	68.9	36.6	17.5	9.2
GeowizardN [FYH ⁺ 24]	UNet	MIX	Block3	6.8	5.4	4.8	6.2	13.0	10.2	6.3	2.7	27.5	17.6	12.0	7.3
GenPercept [XGL ⁺ 24]	UNet	MIX	Block0	21.5	9.6	7.0	16.0	22.7	16.1	7.1	1.8	84.4	40.8	17.3	8.0
GenPercept [XGL ⁺ 24]	UNet	MIX	Block1	62.0	41.9	34.4	52.2	55.7	46.4	27.8	6.4	94.5	64.9	29.7	13.3
GenPercept [XGL ⁺ 24]	UNet	MIX	Block2	28.2	16.4	13.3	22.9	54.9	43.0	23.8	6.1	84.5	45.1	21.5	10.8
GenPercept [XGL ⁺ 24]	UNet	MIX	Block3	8.0	5.9	5.9	7.0	26.6	19.0	10.6	3.8	58.3	31.4	17.4	10.0

Infinigen [RLM⁺23] generates diverse high-quality 3D synthetic scene data, which offers broad coverage of objects and scenes in the natural world with natural phenomena. The surface normal is rendered based on Blender.

MuSHRoom [RWC⁺24] is an indoor real-world multi-sensor hybrid room dataset, which contains 10 rooms captured by Kinect, iPhone, and Faro scanner. We use the ground-truth normal annotations supported by gaustudio [YNC⁺24].

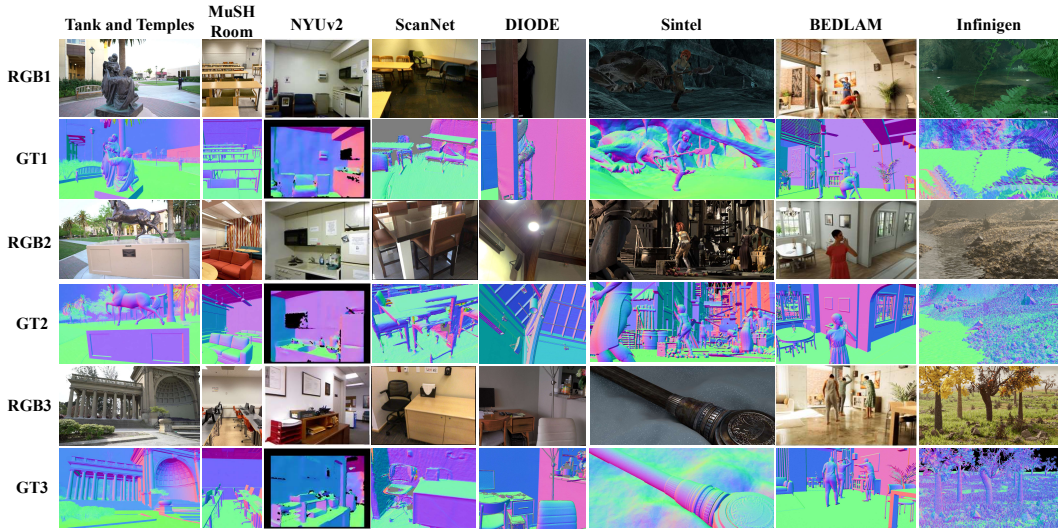


Figure 9: Visualization of the ground-truth surface normal from different datasets.

Tank and Temples (T&T) [KPZK17] is a dataset including both outdoor scenes and indoor environments, whose ground-truth data is captured using an industrial laser scanner. We use the ground-truth normal annotations supported by gaustudio [YNC⁺24].

A.5 Limitations and Future Works

The discussion of monocular depth estimation in this work is limited to single-image monocular affine-invariant depth estimation. Monocular metric depth estimation and video geometry estimation are also important topics, we leave them for future exploration.

A.6 Broader Impacts

In this section, we aim to discuss the potential societal impacts. The positive societal impacts encompass two aspects. First, it helps the research community gain in-depth knowledge about monocular geometry estimation, including performance comparisons between different models, technical details of current models, and future approaches. The release of this work also helps researchers perform experiments to evaluate their methods more comprehensively, fairly, and conveniently. Furthermore, it will significantly boost the progress of downstream tasks. As we mentioned in the paper, monocular geometry estimation can be applied to many downstream tasks, thereby accelerating their progress. In summary, we believe this work will have substantial positive effects on the research community, enriching the capacity of current and future applications and products, and ultimately improving people’s lives. We also evaluated the negative societal impacts and found none.

Acknowledgements: This work was supported by National Key R&D Program of China (No. 2022ZD0118700).

References

- [BD24] Gwangbin Bae and Andrew J. Davison. Rethinking inductive biases for surface normal estimation. In *IEEE/CVF Conference on Computer Vision and Pattern Recognition (CVPR)*, 2024.
- [BPTY23] Michael J. Black, Priyanka Patel, Joachim Tesch, and Jinlong Yang. BEDLAM: A synthetic dataset of bodies exhibiting detailed lifelike animated motion. In *Proceedings IEEE/CVF Conf. on Computer Vision and Pattern Recognition (CVPR)*, pages 8726–8737, June 2023.
- [BRM⁺24] Mohamed El Banani, Amit Raj, Kevis-Kokitsi Maninis, Abhishek Kar, Yuanzhen Li, Michael Rubinstein, Deqing Sun, Leonidas Guibas, Justin Johnson, and Varun Jampani. Probing the 3d awareness of visual foundation models. *arXiv preprint arXiv:2404.08636*, 2024.
- [BWM23] Reiner Birkel, Diana Wofk, and Matthias Müller. Midas v3.1 – a model zoo for robust monocular relative depth estimation. *arXiv preprint arXiv:2307.14460*, 2023.
- [BWSB12] Daniel J Butler, Jonas Wulff, Garrett B Stanley, and Michael J Black. A naturalistic open source movie for optical flow evaluation. In *Proceedings of the European Conference on Computer Vision (ECCV), Part VI*, pages 611–625, 2012.
- [Can86] John Canny. A computational approach to edge detection. *IEEE Trans. Pattern Anal. Mach. Intell.*, pages 679–698, 1986.
- [DBK⁺20] Alexey Dosovitskiy, Lucas Beyer, Alexander Kolesnikov, Dirk Weissenborn, Xiaohua Zhai, Thomas Unterthiner, Mostafa Dehghani, Matthias Minderer, Georg Heigold, Sylvain Gelly, et al. An image is worth 16x16 words: Transformers for image recognition at scale. *arXiv preprint arXiv:2010.11929*, 2020.
- [DCS⁺17] Angela Dai, Angel X Chang, Manolis Savva, Maciej Halber, Thomas Funkhouser, and Matthias Nießner. Scannet: Richly-annotated 3d reconstructions of indoor scenes. In *IEEE Conf. Comput. Vis. Pattern Recog.*, pages 5828–5839, 2017.
- [DDS⁺09] Jia Deng, Wei Dong, Richard Socher, Li-Jia Li, Kai Li, and Li Fei-Fei. Imagenet: A large-scale hierarchical image database. In *2009 IEEE conference on computer vision and pattern recognition*, pages 248–255. Ieee, 2009.
- [DHY⁺20] Mingyu Ding, Yuqi Huo, Hongwei Yi, Zhe Wang, Jianping Shi, Zhiwu Lu, and Ping Luo. Learning depth-guided convolutions for monocular 3D object detection. In *IEEE Conf. Comput. Vis. Pattern Recog. Worksh.*, pages 1000–1001, 2020.
- [DLZR22] Kangle Deng, Andrew Liu, Jun-Yan Zhu, and Deva Ramanan. Depth-supervised NeRF: Fewer views and faster training for free. In *IEEE Conf. Comput. Vis. Pattern Recog.*, pages 12882–12891, 2022.
- [DOMB23] Timothée Darcet, Maxime Oquab, Julien Mairal, and Piotr Bojanowski. Vision transformers need registers, 2023.
- [DT20] Maximilian Denninger and Rudolph Triebel. 3D scene reconstruction from a single viewport. In *Eur. Conf. Comput. Vis.*, pages 51–67. Springer, 2020.
- [ECA⁺23] Patrick Esser, Johnathan Chiu, Parmida Atighehchian, Jonathan Granskog, and Anastasis Germanidis. Structure and content-guided video synthesis with diffusion models. In *Int. Conf. Comput. Vis.*, pages 7346–7356, 2023.
- [EKB⁺24] Patrick Esser, Sumith Kulal, Andreas Blattmann, Rahim Entezari, Jonas Müller, Harry Saini, Yam Levi, Dominik Lorenz, Axel Sauer, Frederic Boesel, et al. Scaling rectified flow transformers for high-resolution image synthesis. *arXiv preprint arXiv:2403.03206*, 2024.

- [EPF14] David Eigen, Christian Puhrsch, and Rob Fergus. Depth map prediction from a single image using a multi-scale deep network. In *Adv. Neural Inform. Process. Syst.*, pages 2366–2374, 2014.
- [FYH⁺24] Xiao Fu, Wei Yin, Mu Hu, Kaixuan Wang, Yuexin Ma, Ping Tan, Shaojie Shen, Dahua Lin, and Xiaoxiao Long. Geowizard: Unleashing the diffusion priors for 3d geometry estimation from a single image. *arXiv preprint arXiv: 2403.12013*, 2024.
- [GFP⁺24] Ming Gui, Johannes S. Fischer, Ulrich Prestel, Pingchuan Ma, Dmytro Kotovenko, Olga Grebenkova, Stefan Andreas Baumann, Vincent Tao Hu, and Björn Ommer. Depthfm: Fast monocular depth estimation with flow matching. *arXiv preprint arXiv: 2403.13788*, 2024.
- [GLU12] Andreas Geiger, Philip Lenz, and Raquel Urtasun. Are we ready for autonomous driving? the kitti vision benchmark suite. In *IEEE Conf. Comput. Vis. Pattern Recog.*, pages 3354–3361, 2012.
- [GMAFB19] Clément Godard, Oisín Mac Aodha, Michael Firman, and Gabriel J Brostow. Digging into self-supervised monocular depth estimation. In *Int. Conf. Comput. Vis.*, pages 3828–3838, 2019.
- [GWCV16] Adrien Gaidon, Qiao Wang, Yohann Cabon, and Eleonora Vig. Virtual worlds as proxy for multi-object tracking analysis. In *IEEE Conf. Comput. Vis. Pattern Recog.*, pages 4340–4349, 2016.
- [HSW⁺21] Edward J Hu, Yelong Shen, Phillip Wallis, Zeyuan Allen-Zhu, Yuanzhi Li, Shean Wang, Lu Wang, and Weizhu Chen. Lora: Low-rank adaptation of large language models. *arXiv preprint arXiv:2106.09685*, 2021.
- [HWSH22] Kuan-Chih Huang, Tsung-Han Wu, Hung-Ting Su, and Winston H Hsu. MonoDTR: Monocular 3D object detection with depth-aware transformer. In *IEEE Conf. Comput. Vis. Pattern Recog.*, pages 4012–4021, 2022.
- [HYZ⁺24] Mu Hu, Wei Yin, Chi Zhang, Zhipeng Cai, Xiaoxiao Long, Hao Chen, Kaixuan Wang, Gang Yu, Chunhua Shen, and Shaojie Shen. Metric3d v2: A versatile monocular geometric foundation model for zero-shot metric depth and surface normal estimation. *arXiv preprint arXiv:2404.15506*, 2024.
- [HZFG19] Jingwei Huang, Yichao Zhou, Thomas Funkhouser, and Leonidas J Guibas. Framenet: Learning local canonical frames of 3d surfaces from a single rgb image. In *Proceedings of the IEEE/CVF International Conference on Computer Vision*, pages 8638–8647, 2019.
- [HZN⁺18] Jingwei Huang, Yichao Zhou, Matthias Niessner, Jonathan Richard Shewchuk, and Leonidas J Guibas. QuadriFlow: A scalable and robust method for quadrangulation. In *Computer Graphics Forum*, volume 37, pages 147–160. Wiley Online Library, 2018.
- [HZY⁺19] Jingwei Huang, Haotian Zhang, Li Yi, Thomas Funkhouser, Matthias Nießner, and Leonidas J Guibas. TextureNet: Consistent local parametrizations for learning from high-resolution signals on meshes. In *Proceedings of the IEEE/CVF Conference on Computer Vision and Pattern Recognition*, pages 4440–4449, 2019.
- [JCX⁺23] Yuanfeng Ji, Zhe Chen, Enze Xie, Lanqing Hong, Xihui Liu, Zhaoqiang Liu, Tong Lu, Zhenguo Li, and Ping Luo. DDP: Diffusion model for dense visual prediction. In *Int. Conf. Comput. Vis.*, pages 21741–21752, 2023.
- [JME⁺24] Varun Jampani, Kevis-Kokitsi Maninis, Andreas Engelhardt, Arjun Karpur, Karen Truong, Kyle Sargent, Stefan Popov, André Araujo, Ricardo Martin Brullalla, Kaushal Patel, et al. Navi: Category-agnostic image collections with high-quality 3d shape and pose annotations. *Advances in Neural Information Processing Systems*, 36, 2024.
- [KLFK18] Tobias Koch, Lukas Liebel, Friedrich Fraundorfer, and Marco Korner. Evaluation of cnn-based single-image depth estimation methods. In *Eur. Conf. Comput. Vis. Worksh.*, 2018.

- [KMR⁺23] Alexander Kirillov, Eric Mintun, Nikhila Ravi, Hanzi Mao, Chloe Rolland, Laura Gustafson, Tete Xiao, Spencer Whitehead, Alexander C. Berg, Wan-Yen Lo, Piotr Dollár, and Ross Girshick. Segment anything. *Int. Conf. Comput. Vis.*, 2023.
- [KOH⁺24] Bingxin Ke, Anton Obukhov, Shengyu Huang, Nando Metzger, Rodrigo Caye Daudt, and Konrad Schindler. Repurposing diffusion-based image generators for monocular depth estimation. In *IEEE Conf. Comput. Vis. Pattern Recog.*, 2024.
- [KPZK17] Arno Knapitsch, Jaesik Park, Qian-Yi Zhou, and Vladlen Koltun. Tanks and temples: Benchmarking large-scale scene reconstruction. *ACM Trans. Graph.*, 36(4):1–13, 2017.
- [KW14] Diederik P. Kingma and Max Welling. Auto-encoding variational bayes. In *Int. Conf. Learn. Represent.*, 2014.
- [LBH15] Yann LeCun, Yoshua Bengio, and Geoffrey Hinton. Deep learning. *Nature*, 521(7553):436–444, 2015.
- [LCBH⁺22] Yaron Lipman, Ricky TQ Chen, Heli Ben-Hamu, Maximilian Nickel, and Matt Le. Flow matching for generative modeling. *arXiv preprint arXiv:2210.02747*, 2022.
- [LJX⁺23] Yixuan Li, Lihan Jiang, Linning Xu, Yuanbo Xiangli, Zhenzhi Wang, Dahua Lin, and Bo Dai. Matrixcity: A large-scale city dataset for city-scale neural rendering and beyond. In *Int. Conf. Comput. Vis.*, pages 3205–3215, 2023.
- [LOM20] Jan Eric Lenssen, Christian Osendorfer, and Jonathan Masci. Deep iterative surface normal estimation. In *IEEE Conf. Comput. Vis. Pattern Recog.*, pages 11247–11256, 2020.
- [LTH⁺23] Simian Luo, Yiqin Tan, Longbo Huang, Jian Li, and Hang Zhao. Latent consistency models: Synthesizing high-resolution images with few-step inference. *arXiv preprint arXiv: 2310.04378*, 2023.
- [LTLY24] Hsin-Ying Lee, Hung-Yu Tseng, Hsin-Ying Lee, and Ming-Hsuan Yang. Exploiting diffusion prior for generalizable dense prediction. In *IEEE Conf. Comput. Vis. Pattern Recog.*, 2024.
- [LZP14] L’ubor Ladický, Bernhard Zeisl, and Marc Pollefeys. Discriminatively trained dense surface normal estimation. In *Eur. Conf. Comput. Vis.*, pages 468–484. Springer, 2014.
- [mad23] madebyollin. Tiny autoencoder for stable diffusion. <https://github.com/madebyollin/taesd>, 2023.
- [ODM⁺24] Maxime Oquab, Timothée Darcet, Théo Moutakanni, Huy Vo, and Marc Szafraniec *et al.* DINOv2: Learning robust visual features without supervision. *Trans. Mach. Learn. Research*, 2024.
- [PEL⁺23] Dustin Podell, Zion English, Kyle Lacey, Andreas Blattmann, Tim Dockhorn, Jonas Müller, Joe Penna, and Robin Rombach. Sdxl: Improving latent diffusion models for high-resolution image synthesis. *arXiv preprint arXiv: 2307.01952*, 2023.
- [RBK21] René Ranftl, Alexey Bochkovskiy, and Vladlen Koltun. Vision transformers for dense prediction. In *Int. Conf. Comput. Vis.*, pages 12179–12188, 2021.
- [RBL⁺22] Robin Rombach, Andreas Blattmann, Dominik Lorenz, Patrick Esser, and Bjorn Ommer. High-resolution image synthesis with latent diffusion models. In *IEEE Conf. Comput. Vis. Pattern Recog.*, 2022.
- [RBM⁺22] Barbara Roessle, Jonathan T Barron, Ben Mildenhall, Pratul P Srinivasan, and Matthias Nießner. Dense depth priors for neural radiance fields from sparse input views. In *IEEE Conf. Comput. Vis. Pattern Recog.*, pages 12892–12901, 2022.

- [RFB15] Olaf Ronneberger, Philipp Fischer, and Thomas Brox. U-net: Convolutional networks for biomedical image segmentation. In *International Conference on Medical Image Computing and Computer Assisted Intervention (MICCAI), Part III*, pages 234–241, 2015.
- [RKH⁺21] Alec Radford, Jong Wook Kim, Chris Hallacy, Aditya Ramesh, Gabriel Goh, Sandhini Agarwal, Girish Sastry, Amanda Askell, Pamela Mishkin, Jack Clark, et al. Learning transferable visual models from natural language supervision. In *Proc. Int. Conf. Mach. Learn.*, pages 8748–8763, 2021.
- [RLH⁺22] René Ranftl, Katrin Lasinger, David Hafner, Konrad Schindler, and Vladlen Koltun. Towards robust monocular depth estimation: Mixing datasets for zero-shot cross-dataset transfer. *IEEE Trans. Pattern Anal. Mach. Intell.*, 44(3), 2022.
- [RLM⁺23] Alexander Raistrick, Lahav Lipson, Zeyu Ma, Lingjie Mei, Mingzhe Wang, Yiming Zuo, Karhan Kayan, Hongyu Wen, Beining Han, Yihan Wang, et al. Infinite photorealistic worlds using procedural generation. In *Proceedings of the IEEE/CVF Conference on Computer Vision and Pattern Recognition*, pages 12630–12641, 2023.
- [RRR⁺21] Mike Roberts, Jason Ramapuram, Anurag Ranjan, Atulit Kumar, Miguel Angel Bautista, Nathan Paczan, Russ Webb, and Joshua M. Susskind. Hypersim: A photo-realistic synthetic dataset for holistic indoor scene understanding. In *International Conference on Computer Vision (ICCV) 2021*, 2021.
- [RWC⁺24] Xuqian Ren, Wenjia Wang, Dingding Cai, Tuuli Tuominen, Juho Kannala, and Esa Rahtu. Mushroom: Multi-sensor hybrid room dataset for joint 3d reconstruction and novel view synthesis. In *Proceedings of the IEEE/CVF Winter Conference on Applications of Computer Vision*, pages 4508–4517, 2024.
- [SHH⁺24] Saurabh Saxena, Charles Herrmann, Junhwa Hur, Abhishek Kar, Mohammad Norouzi, Deqing Sun, and David J Fleet. The surprising effectiveness of diffusion models for optical flow and monocular depth estimation. *Adv. Neural Inform. Process. Syst.*, 36, 2024.
- [SHKF12] Nathan Silberman, Derek Hoiem, Pushmeet Kohli, and Rob Fergus. Indoor segmentation and support inference from rgb-d images. In *Proceedings of the European Conference on Computer Vision (ECCV), Part V*, pages 746–760, 2012.
- [SMP⁺20] Shreeyak Sajjan, Matthew Moore, Mike Pan, Ganesh Nagaraja, Johnny Lee, Andy Zeng, and Shuran Song. Clear grasp: 3d shape estimation of transparent objects for manipulation. In *2020 IEEE International Conference on Robotics and Automation (ICRA)*, pages 3634–3642. IEEE, 2020.
- [SSG⁺17] Thomas Schops, Johannes L Schonberger, Silvano Galliani, Torsten Sattler, Konrad Schindler, Marc Pollefeys, and Andreas Geiger. A multi-view stereo benchmark with high-resolution images and multi-camera videos. In *IEEE Conf. Comput. Vis. Pattern Recog.*, pages 3260–3269, 2017.
- [SXC⁺21] Jiaming Sun, Yiming Xie, Linghao Chen, Xiaowei Zhou, and Hujun Bao. NeuralRecon: Real-time coherent 3d reconstruction from monocular video. In *IEEE Conf. Comput. Vis. Pattern Recog.*, pages 15598–15607, 2021.
- [SYX⁺22] Libo Sun, Wei Yin, Enze Xie, Zhengrong Li, Changming Sun, and Chunhua Shen. Improving monocular visual odometry using learned depth. *IEEE Trans. Robot.*, 38(5):3173–3186, 2022.
- [TL19] Mingxing Tan and Quoc Le. Efficientnet: Rethinking model scaling for convolutional neural networks. In *International conference on machine learning*, pages 6105–6114. PMLR, 2019.
- [TTLN17] Keisuke Tateno, Federico Tombari, Iro Laina, and Nassir Navab. CNN-SLAM: Real-time dense monocular slam with learned depth prediction. In *IEEE Conf. Comput. Vis. Pattern Recog.*, pages 6243–6252, 2017.

- [VKZ⁺19] Igor Vasiljevic, Nick Kolkin, Shanyi Zhang, Ruotian Luo, Haochen Wang, Falcon Z. Dai, Andrea F. Daniele, Mohammadreza Mostajabi, Steven Basart, Matthew R. Walter, and Gregory Shakhnarovich. DIODE: A Dense Indoor and Outdoor DEpth Dataset. *arXiv: Comp. Res. Repository*, 2019.
- [WDH⁺23] Sanghyun Woo, Shoubhik Debnath, Ronghang Hu, Xinlei Chen, Zhuang Liu, In So Kweon, and Saining Xie. Convnext v2: Co-designing and scaling convnets with masked autoencoders. In *Proceedings of the IEEE/CVF Conference on Computer Vision and Pattern Recognition*, pages 16133–16142, 2023.
- [WFG15] Xiaolong Wang, David Fouhey, and Abhinav Gupta. Designing deep networks for surface normal estimation. In *IEEE Conf. Comput. Vis. Pattern Recog.*, pages 539–547, 2015.
- [WGH⁺23] Cho-Ying Wu, Quankai Gao, Chin-Cheng Hsu, Te-Lin Wu, Jing-Wen Chen, and Ulrich Neumann. Inspacetype: Reconsider space type in indoor monocular depth estimation. *arXiv preprint arXiv:2309.13516*, 2023.
- [WYK⁺20] Xinlong Wang, Wei Yin, Tao Kong, Yuning Jiang, Lei Li, and Chunhua Shen. Task-aware monocular depth estimation for 3D object detection. In *AAAI*, volume 34, pages 12257–12264, 2020.
- [WZW⁺20] Wenshan Wang, DeLong Zhu, Xiangwei Wang, Yaoyu Hu, Yuheng Qiu, Chen Wang, Yafei Hu, Ashish Kapoor, and Sebastian Scherer. Tartanair: A dataset to push the limits of visual slam. In *2020 IEEE/RSJ International Conference on Intelligent Robots and Systems (IROS)*, pages 4909–4916. IEEE, 2020.
- [XGL⁺24] Guangkai Xu, Yongtao Ge, Mingyu Liu, Chengxiang Fan, Kangyang Xie, Zhiyue Zhao, Hao Chen, and Chunhua Shen. Diffusion models trained with large data are transferable visual models. *arXiv preprint arXiv: 2403.06090*, 2024.
- [YKH⁺24] Lihe Yang, Bingyi Kang, Zilong Huang, Xiaogang Xu, Jiashi Feng, and Hengshuang Zhao. Depth anything: Unleashing the power of large-scale unlabeled data. In *IEEE Conf. Comput. Vis. Pattern Recog.*, 2024.
- [YLL⁺20] Yao Yao, Zixin Luo, Shiwei Li, Jingyang Zhang, Yufan Ren, Lei Zhou, Tian Fang, and Long Quan. Blendedmvs: A large-scale dataset for generalized multi-view stereo networks. *Computer Vision and Pattern Recognition (CVPR)*, 2020.
- [YNC⁺24] Chongjie Ye, Yinyu Nie, Jiahao Chang, Yuantao Chen, Yihao Zhi, and Xiaoguang Han. Gaustudio: A modular framework for 3d gaussian splatting and beyond. *arXiv preprint arXiv:2403.19632*, 2024.
- [YSWC20] Nan Yang, Lukas von Stumberg, Rui Wang, and Daniel Cremers. D3VO: Deep depth, deep pose and deep uncertainty for monocular visual odometry. In *IEEE Conf. Comput. Vis. Pattern Recog.*, pages 1281–1292, 2020.
- [YWSC18] Nan Yang, Rui Wang, Jorg Stuckler, and Daniel Cremers. Deep virtual stereo odometry: Leveraging deep depth prediction for monocular direct sparse odometry. In *Eur. Conf. Comput. Vis.*, pages 817–833, 2018.
- [YZC⁺23] Wei Yin, Chi Zhang, Hao Chen, Zhipeng Cai, Gang Yu, Kaixuan Wang, Xiaozhi Chen, and Chunhua Shen. Metric3d: Towards zero-shot metric 3d prediction from a single image. In *Int. Conf. Comput. Vis.*, 2023.
- [ZBSL17] Tinghui Zhou, Matthew Brown, Noah Snavely, and David Lowe. Unsupervised learning of depth and ego-motion from video. In *IEEE Conf. Comput. Vis. Pattern Recog.*, pages 1851–1858, 2017.
- [ZCC⁺24] Shihao Zhao, Dongdong Chen, Yen-Chun Chen, Jianmin Bao, Shaozhe Hao, Lu Yuan, and Kwan-Yee K Wong. Uni-ControlNet: All-in-one control to text-to-image diffusion models. *Adv. Neural Inform. Process. Syst.*, 36, 2024.

- [ZRA23] Lvmin Zhang, Anyi Rao, and Maneesh Agrawala. Adding conditional control to text-to-image diffusion models. In *Proceedings of the IEEE/CVF International Conference on Computer Vision*, pages 3836–3847, 2023.
- [ZRL⁺23] Wenliang Zhao, Yongming Rao, Zuyan Liu, Benlin Liu, Jie Zhou, and Jiwen Lu. Unleashing text-to-image diffusion models for visual perception. In *Int. Conf. Comput. Vis.*, pages 5729–5739, 2023.